ELSEVIER

Nuclear Instruments and Methods in Physics Research B 181 (2001) 219–224

NIM B
Beam Interactions with Materials & Atoms

www.elsevier.com/locate/nimb

Imaging of charge transport properties in polycrystalline CVD diamond using IBIC and IBIL microscopy

M.B.H. Breese [a,*], P.J. Sellin [a], L.C. Alves [b,c], A.P. Knights [d], R.S. Sussmann [e], A.J. Whitehead [e]

[a] *Department of Physics, School of Physical Sciences, University of Surrey, Guildford, GU2 5XH, UK*
[b] *ITN, Dep. Física, EN10, 2686-953 Sacavém, Portugal*
[c] *CFNUL, Av. Prof. Gama Pinto 2, 1699 Lisbon, Portugal*
[d] *Department of Electronic and Electrical Engineering, University of Surrey, Guildford, UK*
[e] *De Beers Industrial Diamonds (UK) Ltd, Ascot, UK*

Abstract

Ion beam induced charge (IBIC) and ion beam induced luminescence (IBIL) results of polycrystalline CVD diamond radiation detectors are presented. These detectors were designed as alpha particle and UV sensors, and were constructed with a coplanar electrode structure, fabricated only on the growth side of the diamond film. IBIC results show the different efficiencies of individual 10–20 μm wide grains at facilitating charge transport at different locations away from the surface metallisation. IBIL results show that some of the large grains which exhibit poor charge collection give a high luminescence yield, whereas other regions exhibit both a low IBIC and IBIL signals. These results directly show that the charge collection efficiency in the inter-electrode region is limited both by the size of the diamond crystallites and also by the high luminescence yield of certain grains.

1. Introduction

Diamond radiation detectors possess a unique combination of electronic and mechanical properties, such as ultra-low room temperature leakage current, radiation hardness, chemical inertness and the ability to operate at high temperature (see, for example, a recent review [1]). Diamond X-ray detectors are also of interest for use in medical dosimetry applications due to their near tissue-equivalence [2]. However, their performance is limited by low charge collection efficiencies due to poor charge transport within the polycrystalline material.

Ion beam induced charge (IBIC) analysis of CVD diamond has been used by Manfredotti et al. [3] to show widely varying charge collection efficiency across the collecting diamond surface, tentatively ascribed to recombination at grain boundaries. A polarisation effect was observed, whereby the measured charge pulse spectrum shifted down in height with cumulative ion dose, due to a build-up of unbound charge within the

* Corresponding author. Tel.: +44-1483-876796; fax: +44-1483-876781.
E-mail address: m.breese@surrey.ac.uk (M.B.H. Breese).

0168-583X/01/$ - see front matter
PII: S0168-583X(01)00536-5

diamond. IBIC analysis, when used in a lateral mode by irradiating a diamond detector along a cleaved cross-section, showed that the collection length increased linearly with sample thickness, in accordance with an increase in grain size as a function of depth throughout the diamond [4]. More recently, the same group combined IBIC with ion beam induced luminescence (IBIL) microscopy to study the distributions of radiative as well as non-radiative recombination centres across large areas of a CVD diamond film [5]. IBIC has also been applied in Melbourne to the study of CVD diamond films, and individual crystal grains were imaged which showed widely differing charge collection efficiencies in adjacent grains [6,7].

Most recently, we have performed IBIC analysis of individual CVD diamond grains in a single-sided radiation detector as part of the development of polycrystalline diamond radiation detectors [8], particularly for use in harsh industrial environments. Good correlation was shown between regions of high measured charge collection and large crystallites as observed in SEM images, and regions of low charge collection corresponding in some cases with regions of small crystallites. This present study develops this analysis further by showing both IBIC and IBIL images of the same regions of these CVD diamond detectors, enabling the radiative and non-radiative behaviour of individual grains to be distinguished.

2. Coplanar CVD diamond detector

Results are presented here from a CVD diamond radiation detector fabricated in a coplanar, or single-sided, geometry. This geometry has been previously described by Bergonzo et al. [9] and exploits the improved charge transport properties observed in CVD diamond at the 'growth' surface, as opposed to the poor charge transport at the 'substrate' surface. This improved charge transport is attributed to the larger size and more regular ordering of the crystallites at the growth surface. Conventionally, ionising radiation detectors have been fabricated from CVD diamond using a sandwich geometry in which the electrical contacts are fabricated on both sides of the diamond film. This sandwich structure produces a uniform electric field through the thickness of the film, however, the effective charge drift lengths in such devices are reduced due to the poor charge collection present in the diamond close to the substrate surface.

The coplanar geometry studied here is realised in a 10 mm × 10 mm sample of undoped polycrystalline CVD diamond film of thickness 70 μm, by fabricating an inter-digitated structure of electrodes acting as ohmic contacts onto the growth surface. The 50 μm wide electrodes were fabricated on the unpolished growth (top) surface of the film using thermally evaporated Cr/Au

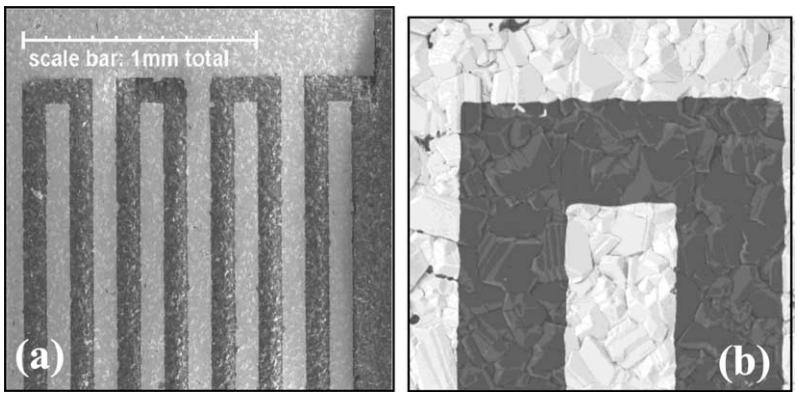

Fig. 1. SEM images of the detector structure. The light regions in the SEM image correspond to the metal electrodes.

contacts and photolithography. Between each electrode was a 50 μm wide inter-electrode gap. No contacts were fabricated onto the substrate (rear) surface. Fig. 1(a) shows a large area SEM of the detector surface, the light areas corresponding to the metallised portions. Fig. 1(b) shows a magnified image of one electrode tip, in which the typical structure of the individual grains can be seen in the inter-electrode gaps and also under the thin metallisation.

The coplanar electrode geometry produces an electric field distribution which is concentrated in the portion of the film close to the top surface, with field lines in the regions between the electrodes lying approximately parallel to the film surface. Consequently the detector is predominantly sensitive to charge transport within the larger, near-surface crystallites. The electric field strength in the regions directly below the metal electrodes will be significantly less than in the inter-electrode active regions, causing greatly reduced charge transport under the metal electrodes.

3. Results

The IBIC and IBIL results were obtained using the Lisbon nuclear microprobe [10] with the conventional IBIC set-up as described in [11]. Fig. 2 shows four IBIC images with increasing magnification of part of the diamond detector, produced using 2 MeV protons which have a range of 24 μm in diamond, and a bias voltage of 200 V on alternate electrodes. The images are slightly skewed owing to the orientation of the microprobe scan coils. The IBIC image in Fig. 2(a) covers an area of 2.5 mm × 2.5 mm, with the detector active area in the lower portion. The vertically running dark regions indicate areas of lowest charge collection efficiency, corresponding to the metal electrodes. The vertically running white regions, showing the largest charge pulse signals, correspond to the exposed diamond between the electrodes, across which the electric field gradient exists. The highest regions of charge collection are concentrated at the tips of each electrode, consistent with the

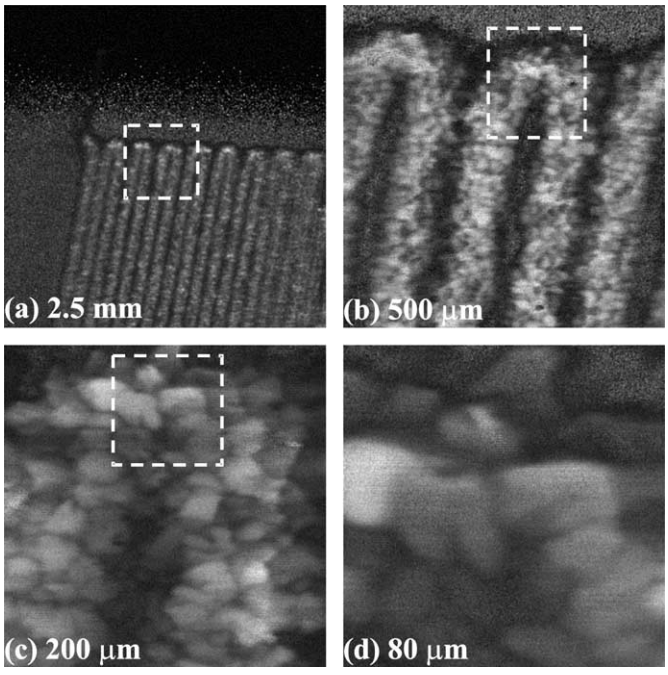

Fig. 2. IBIC images acquired using 2 MeV protons showing increasing magnification of a region at the tip of a single electrode at bias voltages of 200 V. Light areas exhibit a high average charge collection and dark areas exhibit a low average charge collection. The images were collected for 20 min each.

geometrical concentration of the electric field at these locations. Non-uniformities in the charge collection efficiency at the tip of the electrode strips can also be seen due to the highly non-uniform electric field profile at these positions.

Fig. 2(b) shows a higher magnification image of the boxed area in Fig. 2(a), and resolved grains are visible as the white areas. Figs. 2(c) and (d) were recorded at greater magnifications, again from the previous boxed area, showing close-ups of the tip of one electrode. Individual, light-coloured crystallites are clearly visible which exhibit high charge collection efficiency, particularly adjacent to the tips of the electrode where the field strength is greater. The dark regions between them are the boundaries between adjacent grains. In Figs. 2(c) and (d), widely differing collection efficiencies are observed in adjacent grains, where the field strength and hence the collection efficiency would be expected to be similar. This can be seen from the different shades of grey of the individual grains.

The IBIC images in Fig. 3 show the effect on the measured charge collection behaviour of increasing the detector bias voltage (within the same area shown in Fig. 2(c)). Since the images were only collected for 5 min each and show the number of counts above threshold, the contrast is inferior to that shown in Fig. 2 [11]. The outline of the metallisation is shown in Fig. 3(a). Charge collection is first observed at the electrode edges, and even at 20 V there is a surprising amount of collection here due to field enhancement at the electrode edges. Charge collection increases with bias voltage, and gradually the gap between the electrodes fills in. At voltages of 180 V and above the whole unmetallised region exhibits good collection and further increases in bias voltage do not significantly improve the uniformity of charge collection.

To study further the observed regions of poor charge collection in these IBIC images, a simple IBIL system was also incorporated on the Lisbon microprobe, comprising a Hamamatsu H3165-10 photomultiplier tube and plastic light pipe. This

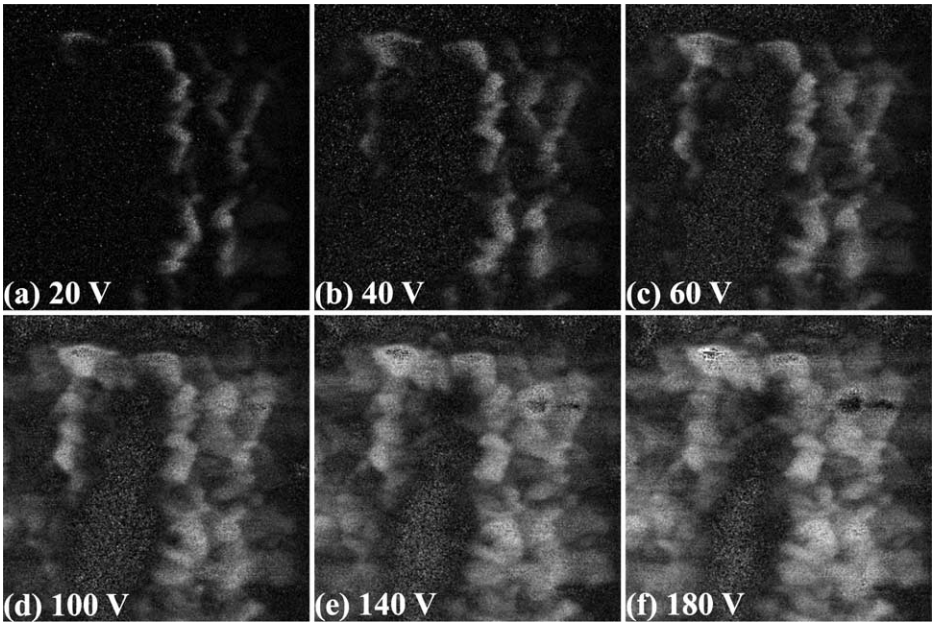

Fig. 3. IBIC images showing the effect of increasing the detector bias voltage from 20 to 180 V. These were acquired using 2 MeV protons from the same 200×200 μm^2 area shown in Fig. 2(c). These images show the total number of counts measured above a threshold on the charge pulse height spectrum. Light areas correspond to a high measured number of pulses and dark areas correspond to a small number of measured pulses. Each image was collected for 5 min.

pointed directly at the sample through the monocular eyepiece of the stereo zoom microscope. The luminescence images were obtained immediately after IBIC analysis of the same area using a higher beam current of 1–10 pA. The IBIL signal strength was not resolved into different wavelength components; only the total light emission was recorded to give an indication of overall luminescence output of adjacent grains. The resultant signal strength was analysed off-line using two or more windows to give an indication of those regions emitting 'dim' light pulses and those regions emitting 'bright' pulses. PIXE images showing the distribution of the gold metallisation was recorded along with the IBIL images, in order to accurately define the electrode edges.

Fig. 4 shows a combination of IBIL, IBIC and PIXE images from a 150×150 μm^2 area around one electrode tip. The PIXE image in Fig. 4(d) shows the metallised electrode portion and the IBIC image in Fig. 4(c), recorded with a bias voltage of 100 V, shows individual grains exhibiting a large charge collection efficiency which are mainly located adjacent to the electrode edges. The IBIL images in Figs. 4(a) and (b) show, respectively, the distribution of dimly emitting and brightly emitting regions within this area, recorded with zero detector bias. There are large regions of dim light emission observed even from under the metallised electrodes, though the intensity is attenuated compared with the non-metallised areas. In Fig. 4(a), approximately 50% of the total area emits dim light, whereas regions which emits bright light in Fig. 4(b) are much smaller, approximately 10–20 μm wide, corresponding to the size of individual grains. None of the regions emitting bright light are located under the metallisation because of its attenuating effect.

The boxed regions in Figs. 4(a)–(c) show different behaviour occurring in different grains. The grain in the centre of the dashed boxes exhibits a strong IBIC signal but no light emission, except

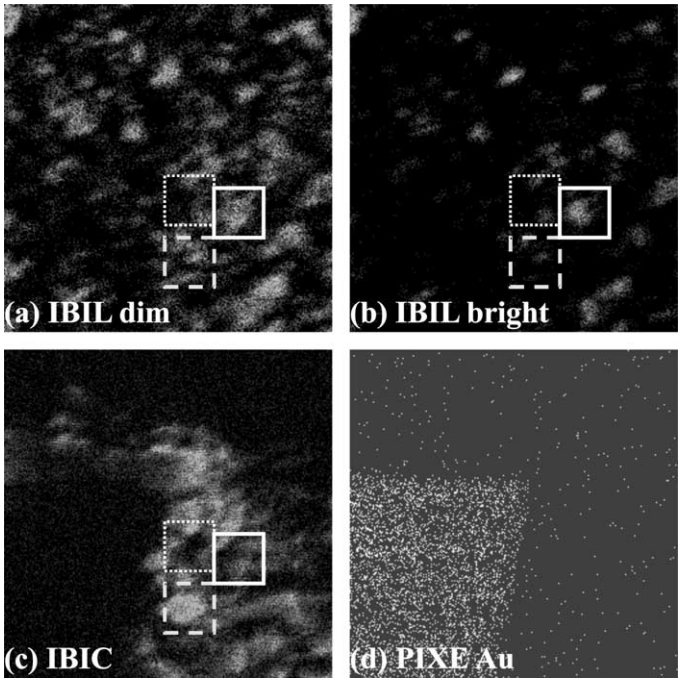

Fig. 4. IBIL, IBIC and PIXE images from a 150×150 μm^2 area of this detector. Light regions represent a high number of counts, and black represents a low count regions. The three types of boxes in the images (a)–(c) correspond to the same area on each image and show different types of behaviour exhibited within this area.

for weak emission at the edges of this grain. The grain in the centre of the boxes enclosed by a solid line exhibits strong light emission, but no charge collection is observed from this grain. The region at the centre, the dotted boxes, shows neither detectable light emission nor charge collection. This area most likely corresponds to agglomerations of very small grains, where the close proximity of grain boundaries produces a short carrier recombination lifetime.

Thus for detector applications, two factors are identified which limit the resultant charge collection efficiency; the presence of clusters of small CVD grains and the tendency of grains to emit light instead of producing a high charge collection. This observation is similar to that made by Manfredotti et al. [3], who recorded large area lateral images showing the complementary behaviour between non-radiative charge collection in IBIC images and radiative luminescence in IBIL images.

4. Conclusions

The charge transport properties of a CVD diamond detector with a coplanar electrode geometry which is predominantly sensitive to charge transport close to the diamond growth surface have been investigated using a combination of IBIC and IBIL. The images show well-resolved, high charge collection efficiency crystallites, with a width of 10–20 μm and other similar size regions exhibiting high luminescence yield. There are also regions which display neither high charge collection nor high luminescence yield, probably corresponding to regions of small crystallites as previously observed [8].

This study emphasises the need for further improvements in the size and quality of the crystallite structure in CVD diamond to enhance the charge transport performance of diamond film for detector applications, and further study of the mechanisms by which individual grains emit light instead of high charge collection. To accomplish this, a wavelength dispersive luminescence system will be used to observe the change in light emission across individual grains and at grain boundaries in this material.

References

[1] W. Adam, Nucl. Instr. and Meth. A 434 (1999) 131.
[2] C.M. Buttar, J. Conway, R. Meyfarth, G. Scarsbrook, P.J. Sellin, A. Whitehead, Nucl. Instr. and Meth. A 392 (1997) 281.
[3] C. Manfredotti, F. Fizotti, E. Vittone, M. Boero, P. Polesello, S. Galassini, M. Jaksic, S. Fazinic, I. Bogdanovic, Nucl. Instr. and Meth. B 100 (1995) 133.
[4] C. Manfredotti, F. Fizotti, E. Vittone, M. Boero, P. Polesello, S. Galassini, M. Jaksic, S. Fazinic, I. Bogdanovic, Nucl. Instr. and Meth. B 109–110 (1996) 552.
[5] C. Manfredotti, F. Fizotti, P. Polesello, E. Vittone, M. Trucatto, A. Lo Giudice, M. Jaksic, P. Rossi, Nucl. Instr. and Meth. B 136–138 (1998) 1333.
[6] D.R. Beckman, A. Saint, P. Gonon, D.N. Jamieson, S. Prawer, R. Kalish, Nucl. Instr. and Meth. B 130 (1997) 518.
[7] D.N. Jamieson, Nucl. Instr. and Meth. B 136–138 (1998) 1.
[8] M.B.H. Breese, P.J. Sellin, L.C. Alves, A.P. Knights, R.S. Sussmann, A.J. Whitehead, Appl. Phys. Lett. 77 (6) (2000) 913.
[9] P. Bergonzo, F. Foulon, R.D. Marshall, C. Jany, A. Brambilla, R.D. McKeag, R.B. Jackman, IEEE Trans. Nucl. Sci. 45 (3) (1998) 370.
[10] L.C. Alves, M.B.H. Breese, E. Alves, A. Paul, M.R. da Silva, M.F. da Silva, J.C. Soares, Nucl. Instr. and Meth. B 161–163 (2000) 334.
[11] M.B.H. Breese, D.N. Jamieson, P.J.C. King, Materials Analysis using a Nuclear Microprobe, Wiley, New York, 1996.